Coactivator SRC-2–dependent metabolic reprogramming mediates prostate cancer survival and metastasis

Subhamoy Dasgupta,[1] Nagireddy Putluri,[1] Weiwen Long,[1] Bin Zhang,[1] Jianghua Wang,[2] Akash K. Kaushik,[1] James M. Arnold,[1] Salil K. Bhowmik,[1] Erin Stashi,[1] Christine A. Brennan,[3] Kimal Rajapakshe,[1] Cristian Coarfa,[1] Nicholas Mitsiades,[1] Michael M. Ittmann,[2,4] Arul M. Chinnaiyan,[3,5,6] Arun Sreekumar,[1] and Bert W. O'Malley[1]

[1]Department of Molecular and Cellular Biology and [2]Department of Pathology and Immunology, Baylor College of Medicine, Houston, Texas, USA. [3]Michigan Center for Translational Pathology, University of Michigan, Ann Arbor, Michigan, USA. [4]Michael E. DeBakey Veterans Affairs Medical Center, Houston, Texas, USA. [5]Department of Pathology and [6]Howard Hughes Medical Institute, University of Michigan, Ann Arbor, Michigan, USA.

Metabolic pathway reprogramming is a hallmark of cancer cell growth and survival and supports the anabolic and energetic demands of these rapidly dividing cells. The underlying regulators of the tumor metabolic program are not completely understood; however, these factors have potential as cancer therapy targets. Here, we determined that upregulation of the oncogenic transcriptional coregulator steroid receptor coactivator 2 (SRC-2), also known as NCOA2, drives glutamine-dependent de novo lipogenesis, which supports tumor cell survival and eventual metastasis. SRC-2 was highly elevated in a variety of tumors, especially in prostate cancer, in which SRC-2 was amplified and overexpressed in 37% of the metastatic tumors evaluated. In prostate cancer cells, SRC-2 stimulated reductive carboxylation of α-ketoglutarate to generate citrate via retrograde TCA cycling, promoting lipogenesis and reprogramming of glutamine metabolism. Glutamine-mediated nutrient signaling activated SRC-2 via mTORC1-dependent phosphorylation, which then triggered downstream transcriptional responses by coactivating SREBP-1, which subsequently enhanced lipogenic enzyme expression. Metabolic profiling of human prostate tumors identified a massive increase in the SRC-2–driven metabolic signature in metastatic tumors compared with that seen in localized tumors, further implicating SRC-2 as a prominent metabolic coordinator of cancer metastasis. Moreover, SRC-2 inhibition in murine models severely attenuated the survival, growth, and metastasis of prostate cancer. Together, these results suggest that the SRC-2 pathway has potential as a therapeutic target for prostate cancer.

Introduction

Tumors scavenge various nutrients for carbon and nitrogen sources required for the synthesis of biomolecules to support the growth and replication of their rapidly dividing cells. Nutrient availability plays a pivotal role in the reprogramming of tumor metabolic pathways to sustain increased energetic and anabolic demands. One of the frequent metabolic adaptations observed in different types of tumor cells is an increased uptake of glucose and aerobic glycolysis, along with decreased oxidative metabolism, a phenomenon widely known as the Warburg effect (1). However, it is well documented that tumor cells do not rely on a single metabolic state but instead acquire a variety of strategies to adapt to alterations in nutrient availability and metabolic stress conditions during the course of disease progression (2, 3). Recent studies using ^{13}C isotopes have identified a complimentary switch of glutamine metabolism by tumor cells to efficiently support carbon utilization for anabolism and growth (4, 5). The glutamine metabolic pathway serves as a crucial source for anaplerosis of carbon atoms to balance the metabolic flux through the TCA cycle and to support the increased biosynthesis of macromolecules, such as nucleotides and lipids, and the synthesis of mitochondrial ATP (6, 7).

Unlike other solid tumors, adenocarcinomas of the prostate display very unique metabolic features, since the majority of primary tumors do not show a classical "glycolytic switch" and so are not efficiently detected in [^{18}F]fluorodeoxyglucose-PET ([^{18}F]FDG-PET) (8). Instead, an aberrant increase in de novo lipogenesis (9), coupled with glucose and glutamine metabolism, is observed (10) in prostatic tumors from early clinical stages and is significantly associated with poor prognosis and worse disease outcome (11). Lipids contribute to various aspects of tumor biology by functioning as building blocks for membrane biogenesis, phospholipids for membrane structure, lipid rafts for cell signaling, and, more important, for energy production and storage (12). While most normal human cells prefer exogenous sources of fatty acids, tumor cells rely more on de novo fatty acid biosynthesis (12), and this is true especially in prostate cancer cells. Thus, it is of utmost importance to identify the oncogenic factors that reprogram the metabolic pathways that maintain this increased lipogenic program in prostate tumors.

Previous findings from our laboratory identified steroid receptor coactivator 2 (SRC-2, also known as NCOA2, TIF2, and GRIP1), a potent transcriptional coregulator for nuclear receptors (NRs) and other transcription factors (13), as a critical coordinator of energy homeostasis (14–17). Importantly, recent findings from

Authorship note: Arun Sreekumar and Bert W. O'Malley contributed equally to this work.
Conflict of interest: The authors have declared that no conflict of interest exists.
Submitted: March 7, 2014; **Accepted:** January 2, 2015.
Reference information: *J Clin Invest*. 2015;125(3):1174–1188. doi:10.1172/JCI76029.

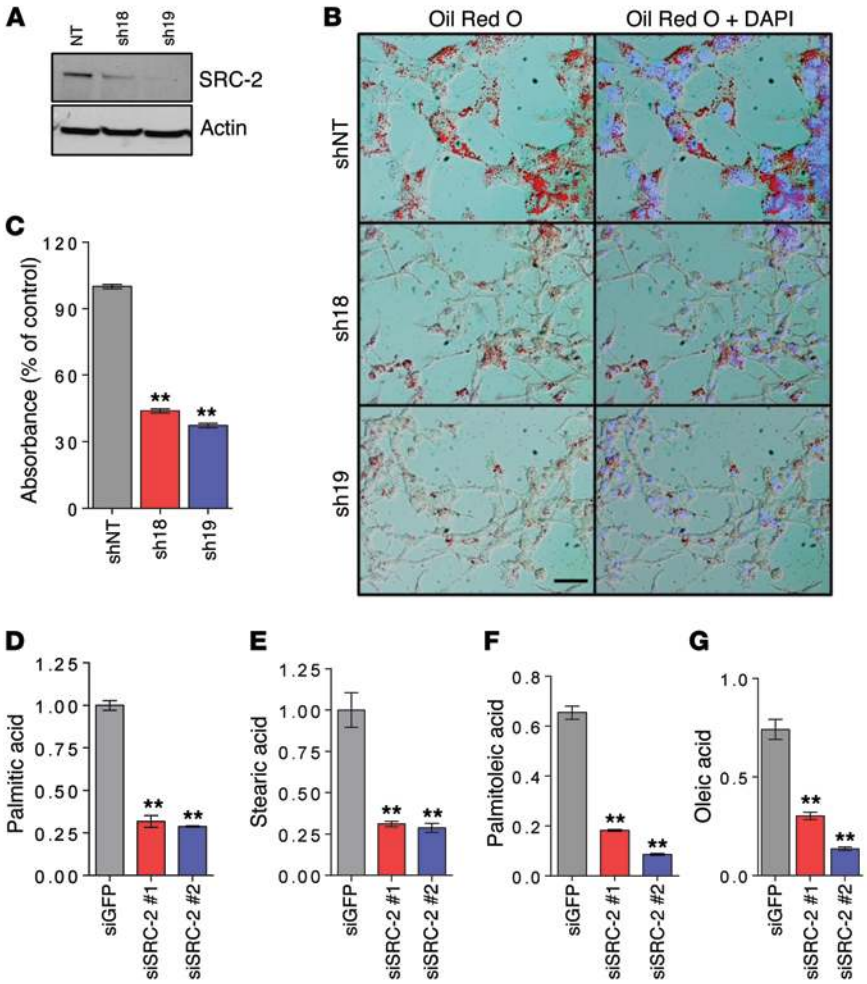

Figure 1. SRC-2 promotes lipogenesis in prostate tumor cells primarily from glutamine sources. (**A**) Western blot showing expression of SRC-2 and actin in C4-2 cells stably expressing shNT and 2 different clones of SRC-2 shRNA (sh18 and sh19). Actin was used to normalize protein loading. The full, uncut gels are shown in the Supplemental Material. (**B**) Oil Red O staining of the stable C4-2 cells shNT, sh18, and sh19 showing the neutral lipid content of the cells. Cells were counterstained with the nuclear marker DAPI, and merged images are shown in the right panels. Scale bar: 10 μm. (**C**) Quantitative analysis of Oil Red O staining by measuring the absorbance (OD at 490 nm) of extracted dye (n = 4). (**D**–**G**) Targeted MS–based metabolomic analyses demonstrating the relative content of palmitic, stearic, palmitoleic, and oleic acids in C4-2 cells treated with control siRNA (siGFP) or 2 different SRC-2 siRNAs (siSRC-2 #1 and siSRC-2 #2) (n = 4/group). Data are represented as the mean ± SEM. $^{**}P < 0.001$ by Student's t test versus shNT or siGFP.

integrative genomic profiling of human prostate tumors revealed that *SRC2* is a potent oncogene in approximately 8% of primary tumors and, notably, in approximately 37% of metastatic prostate tumors (18). Furthermore, prostate cancer patients harboring *SRC2* gene amplification or overexpression had higher rates of biochemical recurrence, and SRC-2 expression was a significant predictor of time-to-biochemical recurrence (19). These findings accentuate the clinical importance of the *SRC2* gene in prostate cancer pathology (20). Functionally, SRC-2 acts as a transcriptional coregulator of androgen receptor (AR) (19) in prostate cancer cells; however, its mode of action in aggressive metastatic castration-resistant prostate cancer (CRPC) is not clearly understood. Moreover, none of the studies have yet investigated the functional role of SRC-2 in cancer metabolism, nor have they determined whether this recent but well-described association of SRC-2 is a critical requirement for prostate cancer cell survival and metastasis (18). In the present study, we sought to identify the molecular functions of SRC-2 as a transcriptional coordinator of tumor metabolism, with the anticipation that these SRC-2–dependent functions could serve as molecular determinants of survival and metastatic competence.

Results

SRC-2 regulates lipogenesis by reductive glutamine metabolism. *Ncoa2* gene deletion studies in mice revealed severe metabolic defects, particularly in fat accretion and energy homeostasis (14–16, 21, 22). Since prostate cancer patients exhibit an increased dependency on fatty acids (23), we first explored the role of SRC-2 in prostate cancer lipogenesis. To assess this, we stably impaired SRC-2 expression using 2 different clones of shRNA (sh18 and sh19) in 3 prostate cancer cell lines: LNCaP (Supplemental Figure 1, A and B; supplemental material available online with this article; doi:10.1172/JCI76029DS1), an androgen-dependent cell line; C4-2 (Figure 1A and Supplemental Figure 1B), an androgen-independent, but responsive, variant of LNCaP that represents the castration-resistant subtype (24, 25); and PC-3 (Supplemental Figure 1, B and C), an AR-negative and highly metastatic line representing aggressive prostate tumors. Oil Red O staining revealed a marked decrease in lipid accumulation due to SRC-2 knockdown in prostate cancer cells (Figure 1, B And C, and Supplemental Figure 1D), and targeted metabolomic analysis identified significantly reduced fatty acid content, both saturated (palmitic and stearic acid) (Figure 1, D and E) and unsaturated (palmitoleic and oleic acids), in the total cellular metabolite pool (Figure 1, F and G). Since glucose oxidation and glutamine metabolism are the 2 major carbon sources for fatty acid synthesis, we compared the relative utilization of glucose and glutamine in prostate cancer cells. C4-2 and PC-3 cells showed higher glutamine consumption compared with that of LNCaP, and SRC-2 ablation significantly reduced glutamine uti-

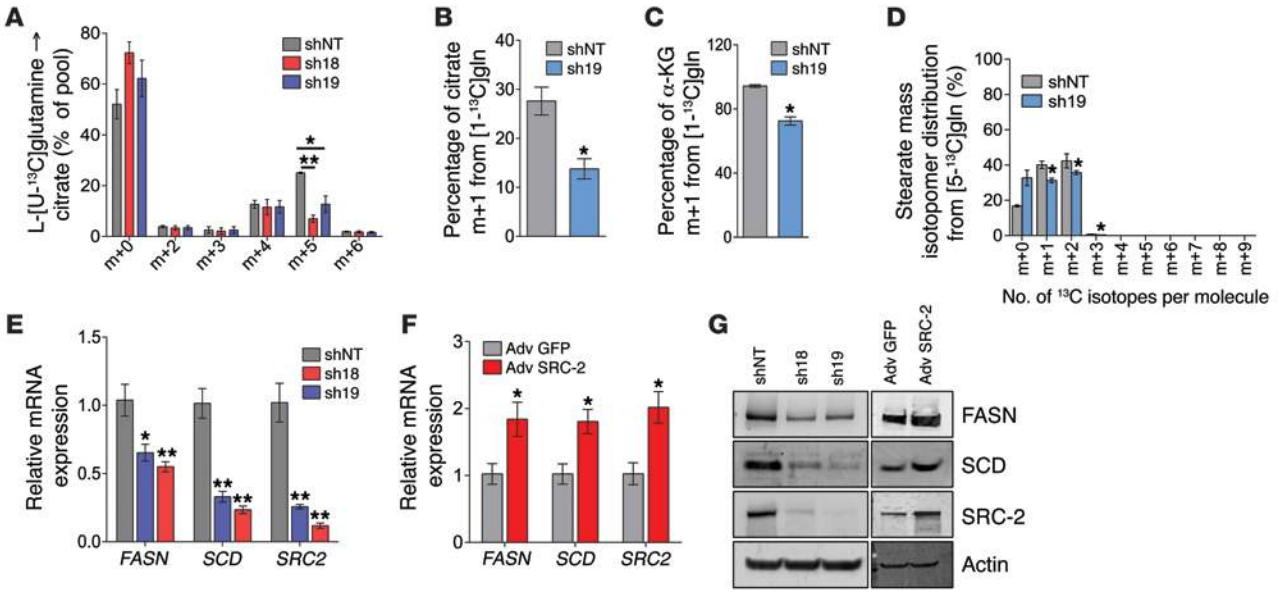

Figure 2. SRC-2 promotes lipogenesis by reductive glutamine metabolism. (**A**) Mass isotopomer distribution of citrate extracted from the stable C4-2 cells shNT (nontargeting) and SRC-2 shRNA clones sh18 and sh19 cultured in the presence of 2 mM L-[U-^{13}C]glutamine and 11 mM unlabeled glucose for 24 hours (n = 6). *P < 0.05 and **P < 0.001 by 2-way ANOVA with Tukey's multiple comparisons test. (**B** and **C**) Citrate and α-ketoglutarate (α-KG) labeling from [1-^{13}C]glutamine ([1-^{13}C]Gln) in the stable C4-2 cells shNT and sh19 (n = 3). (**D**) Mass isotopomer distribution of stearate labeling from [5-^{13}C]glutamine ([5-^{13}C]Gln) in the stable C4-2 cells shNT and sh19 (n = 3). The mass spectrometric method used in this study failed to detect higher fatty acid isotopomers. *P < 0.05 by Student's t test with Holm-Sidak multiple comparisons test. (**E**) qRT-PCR analysis of *FASN*, *SCD*, and *SRC2* gene expression in the stable C4-2 cells shNT, sh18, and sh19 (n = 4). Relative mRNA expression was normalized to actin (housekeeping gene). (**F**) qRT-PCR analysis of *FASN*, *SCD*, and *SRC2* gene expression in C4-2 cells expressing GFP (Adv GFP) and SRC-2 (Adv SRC-2) adenovirus (n = 3). Relative mRNA expression was normalized to actin (housekeeping gene). (**G**) Western blot analysis of FASN, SCD, and SRC-2 in the stable C4-2 cells shNT, sh18, and sh19 and in C4-2 cells expressing GFP adenovirus or SRC-2 adenovirus (n = 3). Actin was used to normalize protein loading. The full, uncut gels are shown in the Supplemental Material. Data are represented as the mean ± SEM. *P < 0.05 and **P < 0.001 by Student's t test (**B**–**F**).

lization in these cells, but not in LNCaP cells (Supplemental Figure 2A). SRC-2 knockdown also showed glucose consumption alterations, albeit minimal (Supplemental Figure 2B) when compared with glutamine utilization (Supplemental Figure 2A).

To understand the biochemical steps affected by loss of SRC-2, we cultured C4-2 cells in the presence of ^{13}C-labeled glucose and glutamine isotopes as tracers followed by tandem mass spectrometry (MS/MS) to measure the enrichment of ^{13}C tracers in intracellular metabolites. C4-2 cells cultured in the presence of uniformly labeled D[U-$^{13}C_6$]glucose showed enrichment of glucose ^{13}C in pyruvate, indicating that the glycolytic pathway is active (Supplemental Figure 2C), but the TCA metabolites such as citrate, α-ketoglutarate, and oxalate failed to show appreciable incorporation of glucose ^{13}C (Supplemental Figure 2C). Similarly, the fatty acids showed minimal enrichment of glucose ^{13}C incorporation (Supplemental Figure 2D), suggesting that there is reduced flow of glucose carbon into the TCA cycle in C4-2 cells. In contrast, uniformly labeled [U-^{13}C]glutamine tracers showed robust enrichment of ^{13}C isotopes in TCA metabolites, and loss of SRC-2 significantly decreased the total percentage of glutamine-derived ^{13}C incorporation in citrate, isocitrate, and α-ketoglutarate (Supplemental Figure 3, A–C). Glutamine (5 carbons) can contribute carbon to citrate (6 carbons) either by oxidative metabolism or by reductive carboxylation to generate citrate (4, 5, 26). The latter reaction requires the addition of an unlabeled carbon to glutamine-derived α-ketoglutarate (5 carbons), generating citrate m+5 (where "m" denotes the nominal mass; m+5 indicates citrate containing 5 additional mass units derived from [U-^{13}C]glutamine) by reversing the enzymatic steps of isocitrate dehydrogenase (IDH) and aconitase (ACO) associated with canonical oxidative TCA. Analysis of citrate isotopomers revealed that loss of SRC-2 expression significantly decreased citrate m+5 levels, with minimal effect on citrate m+4 levels (generated by oxidative TCA) (Figure 2A), indicating that SRC-2 regulates the reductive carboxylation pathway. Supporting this observation, we identified reduced malate and fumarate m+3 levels in SRC-2–depleted C4-2 cells, which are derivatives of citrate m+5, supporting the role of SRC-2 in reductive glutamine metabolism (Supplemental Figure 3D). In addition, [1-^{13}C]glutamine labeling provides a more accurate measurement of reductive carboxylation of α-ketoglutarate to citrate, since this carbon is lost as carbon dioxide by α-ketodehydrogenase in the oxidative pathway but is retained if reductive carboxylation is active (27). By culturing stable C4-2 cells supplemented with [1-^{13}C]glutamine as tracers, we identified the enrichment of citrate m+1 in control cells expressing nontargeting shRNA (shNT), whereas ablation of SRC-2 showed a significant and robust decrease in the percentage of citrate m+1 (Figure 2B). In addition, SRC-2 knockdown also decreased the levels of α-ketoglutarate m+1 (Figure 2C), confirming that SRC-2 regulates the flow of carbon from glutamine to promote the reductive carboxylation of α-ketoglutarate in prostate cancer cells.

Next, we investigated the contribution of reductive carboxylation of glutamine-derived α-ketoglutarate to lipogenesis. To trace

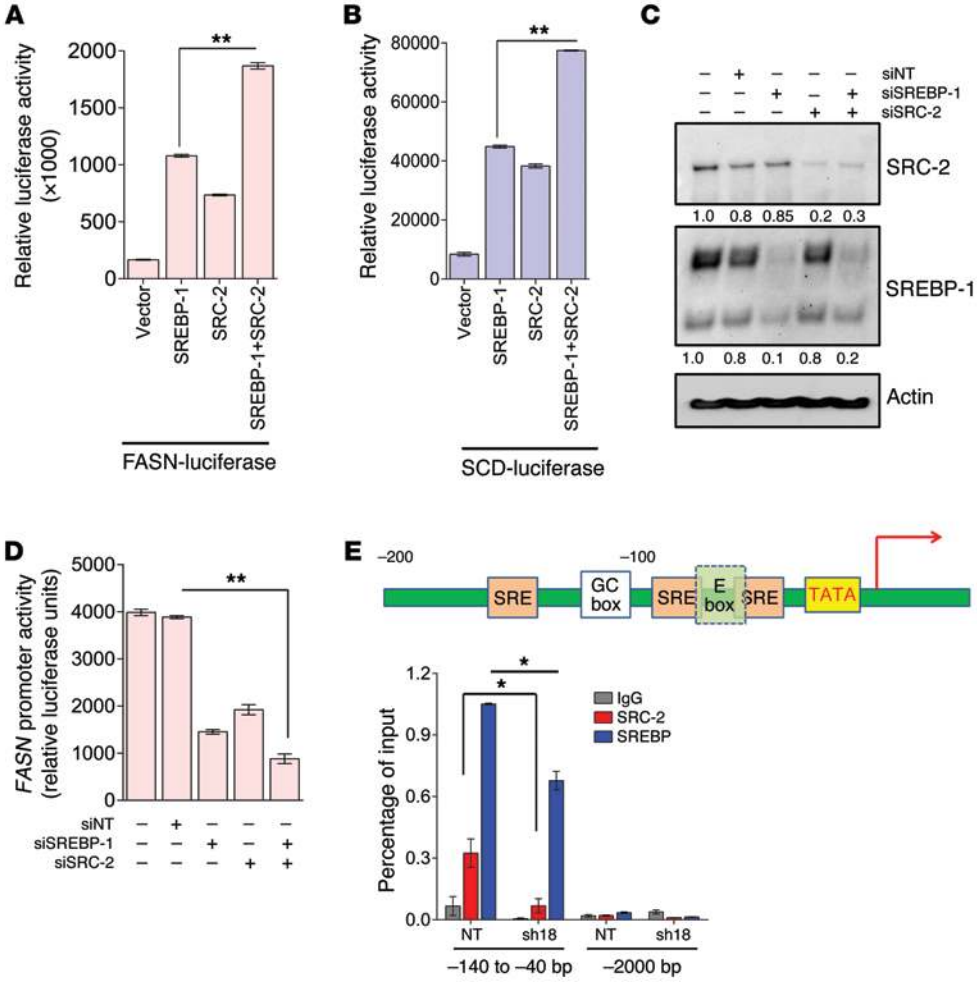

Figure 3. SRC-2 coactivates SREBP1 to promote lipogenesis. (**A**) Luciferase reporter assay in HeLa cells transiently transfected with a FASN-luciferase construct (–220 to +25 bp) in the presence of vector alone, SREBP-1, SRC-2, or a combination of both SRC-2 and SREBP-1 (n = 6). (**B**) Luciferase reporter assay in HeLa cells transiently transfected with an SCD-luciferase construct (–1,280 to +174 bp) in the presence of vector alone, SREBP-1, SRC-2, or a combination of both SRC-2 and SREBP-1 (n = 6). (**C** and **D**) Western blot analysis followed by luciferase reporter assay in PC-3 cells transfected with an FASN-luciferase construct in the presence of control siRNA (siNT), SRC-2-siRNA (siSRC-2), SREBP-1 siRNA (siSREBP-1), or a combination of both SRC-2 and SREBP-1. Semiquantitative levels of each band were analyzed by densitometry using UVP Vision Works LS software, and the relative values (compared with untreated) normalized to actin are indicated numerically under each lane. The full, uncut gels are shown in the Supplemental Material. (**E**) ChIP of SRC-2 and SREBP-1 from the stable C4-2 cells shNT and sh18 showing the recruitment of these 2 proteins on the *FASN* promoter. The amplicons tested were either from a proximal promoter region (–140 to –40 bp) or an unconserved upstream region (–2,000 bp) from the transcriptional start site. IgG antibody was used as a control, and data are presented as a percentage of input chromatin (n = 4). Schematic shows the SRE, GC box, E box, and TATA elements on the *FASN* promoter. Data represent the mean ± SEM. *P < 0.05 by 2-way ANOVA with Tukey's multiple comparisons test (**E**) and **P < 0.001 by Student's t test (**A**, **B**, and **D**).

this, we labeled the stable C4-2 cells with [5-^{13}C]glutamine tracer, since the [1-^{13}C]glutamine-derived isotopic label cannot be incorporated into acetyl-CoA through reductive carboxylation. [5-^{13}C]glutamine transfers only one ^{13}C atom to acetyl-CoA and fatty acids through reductive carboxylation, but loses the ^{13}C incorporation into the acetyl-CoA carbon skeleton via the oxidative pathway. Consequently, [5-^{13}C]glutamine is specific for tracing the reductive carboxylation to the lipid flux (28). Labeling of C4-2 cells with [5-^{13}C]glutamine indicated that reductive carboxylation contributed to the flow of carbon from glutamine to fatty acids, and loss of SRC-2 significantly decreased the mass isotopomer distribution of the fatty acids such as stearate (Figure 2D), palmitate, and oleate (Supplemental Figure 3, E and F). These findings indicate that glutamine contributes to de novo lipogenesis in prostate cancer cells via reductive carboxylation and that SRC-2 plays a key role in regulating the process.

Transcriptional reprogramming supports lipogenesis. To understand the mechanism of SRC-2–dependent lipogenesis in prostate cancer cells, we performed targeted gene expression analysis by quantitative real-time PCR (qRT-PCR) of enzymes (derived from KEGG) involved in glucose and lipid metabolism, the TCA cycle, and glutamine metabolism. SRC-2 depletion had a broad impact on the expression of metabolic genes, among which 2 genes — fatty acid synthase (*FASN*) and stearoyl-CoA desaturase (*SCD*) — were significantly reduced upon SRC-2 silencing (Supplemental Table 1). FASN is a multifunctional enzyme that catalyzes the biosynthesis of long-chain fatty acids from acetyl-CoA and malonyl-CoA, whereas SCD is a desaturase enzyme that synthesizes unsaturated fatty acids by incorporating double bonds into the long-chain fatty acids (11). FASN and SCD have been implicated in the progression of various types of malignancies including prostate cancer (11), but the precise mechanism regulating their increased expression in cancer cells is less understood. We found loss and gain of expression of SRC-2–altered FASN and SCD levels in prostate cancer cells (Figure 2, E–G, and Supplemental Figure 4, A–D), so we undertook to further define the role of SRC-2 in the transcriptional regulation of these 2 genes. Although, SRC-2 is known to be a coactivator of the AR, we observed SRC-2–dependent transcriptional regulation of FASN and SCD in both AR-positive (LNCaP and C4-2) and AR-negative cells (PC-3). To gain further insight into this, we investigated the enrichment of androgen-regulated genes in an LNCaP-siSRC2 gene signature using the gene set enrichment analysis (GSEA) method. We compared the LNCaP-siSRC2 gene signature with an androgen-induced (100 nM DHT) gene signa-

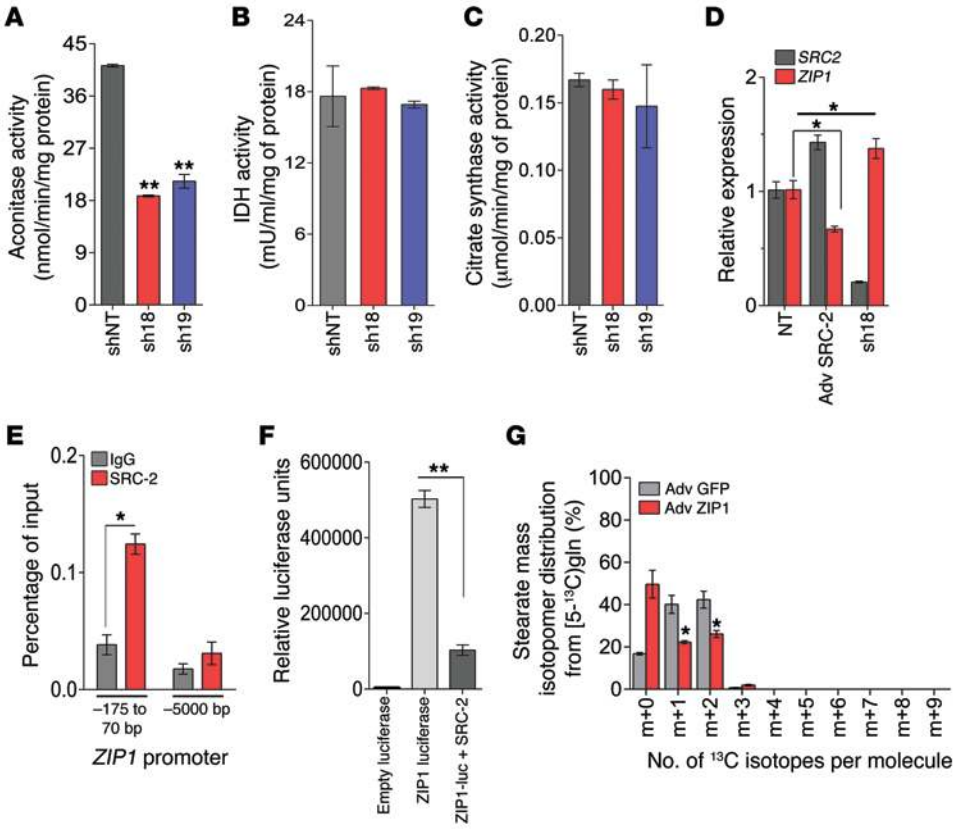

Figure 4. SRC-2 represses transcription of the zinc transporter ZIP1 to stimulate ACO activity. (**A**–**C**) Enzymatic activity of ACO, IDH, and CS in the stable C4-2 cells shNT, sh18, and sh19 (n = 5). (**D**) qRT-PCR analysis of *SRC2* and *ZIP1* (*SLC39A1*) gene expression in the stable C4-2 cells shNT and sh18 and in C4-2 shNT cells expressing SRC-2 adenovirus (n = 4/group). *P < 0.05 by 2-way ANOVA with Tukey's multiple comparisons test. (**E**) ChIP of SRC-2 from C4-2 cells showing the recruitment of SRC-2 on the *ZIP1* proximal promoter (–175 to 70 bp) compared with the –5,000 bp upstream region from the start site. (**F**) Luciferase reporter assay in HeLa cells transiently transfected with empty pGL3 vector (Empty luciferase) and a pGL3-ZIP1-luciferase construct (–246 to +82 bp) in the presence of vector alone (ZIP1 luciferase) or of the SRC-2 construct (ZIP1-luc + SRC-2) (n = 6). (**G**) Mass isotopomer distribution of stearate labeling from [5-^{13}C]glutamine in C4-2 cells ectopically expressing human ZIP1 (Adv ZIP1) or control virus (Adv GFP) (n = 3). The mass spectrometric method used in this study failed to detect higher fatty acid isotopomers. Data represent the mean ± SEM. *P < 0.05 and **P < 0.001 by Student's t test (**A**, **E**, and **F**), with Holm-Sidak multiple comparisons test in **G**.

ture in LNCaP cells (29) and also with an LNCaP-siAR gene signature. The siSRC2-regulated genes did not enrich for either the androgen-induced gene signature (normalized enrichment score [NES] = –0.87, q = 1) or for the siAR response signature (NES = –0.9, q = 0.95) (Supplemental Figure 5, A and B). In contrast, the androgen-induced gene signature was enriched significantly in the siAR gene signature (NES = –2.99, q < 0.001) (Supplemental Figure 5C). These data support the notion that SRC-2 is not acting wholly via the AR, and its association with other transcription factors likely explains why SRC-2 is overexpressed to such a high level in aggressive prostate cancer.

Analysis of SRC-2 ChIP-sequencing (ChIP-seq) data (17) revealed increased occupancy of SRC-2 on the *FASN* and *SCD* promoters, which overlapped with sterol regulatory element–binding protein 1 (SREBP-1) sterol regulatory elements (SREs) in the proximal promoter region (30). To directly test the effects of SRC-2 and SREBP-1 on *FASN* and *SCD* expression, we performed luciferase reporter gene assays using *FASN* (–220 to +25 bp) (31) and *SCD* (–1,280 to +174 bp) promoter constructs. Fitting with the effects observed for endogenous FASN and SCD expression, SRC-2 strongly activated the transcription at both promoters and more so in combination with the SREBP-1 transcription factor (Figure 3, A and B). However, the AR either alone or in combination with SRC-2 failed to activate the luciferase-driven *FASN* promoter in AR-negative PC-3 cells, again indicating that SRC-2 is acting independently of the AR (Supplemental Figure 5D). Similarly, silencing of SRC-2 either alone or in combination with SREBP-1 (Figure 3C) greatly impaired the *FASN* promoter activity in PC-3 cells (Figure 3D), suggesting that SRC-2 coactivates the transcriptional activity of SREBP-1 on the *FASN* and *SCD* promoters. Finally, ChIP assays confirmed strong occupancy of SRC-2 and SREBP-1 on the proximal *FASN* promoter compared with what was detected in the unconserved upstream region (Figure 3E). Interestingly, ablation of SRC-2 showed a modest decrease in the occupancy of SREBP-1 on the *FASN* promoter (Figure 3E), which suggests that recruitment of SRC-2 as a coactivator may facilitate stabilization of SREBP-1 on the chromatin. Together, these data confirm that SRC-2 transcriptionally regulates fatty acid biosynthetic genes primarily by coactivating SREBP-1, independently of the AR.

SRC-2 represses zinc transporter ZIP1 (SLC39A1) to activate ACO enzymatic activity. Next, we investigated the mechanisms by which SRC-2 promotes reductive carboxylation of α-ketoglutarate to generate citrate as indicated by the isotope-labeling studies. Gene expression analysis of enzymes generating citrate from glutamine metabolism did not show any significant alterations upon SRC-2 depletion (Supplemental Figure 6A). Surprisingly, however, we observed a dramatic decrease in ACO enzymatic activity (Figure 4A), but not IDH or citrate synthase (CS) activity (Figure 4, B and C, and ref. 32), in SRC-2–depleted C4-2 cells compared with control C4-2 cells. ACO catalyzes the stereo-specific isomerization of citrate to isocitrate via *cis*-aconitate, and this reversible reaction is allosterically regulated by the intracellular zinc concentration (33). Interestingly, in normal prostate epithelial cells, ACO activity is impaired due to increased amounts of zinc, whereas in prostate tumor cells, this blockage is reversed due to loss of the zinc transporter ZIP1 (SLC39A1) (34). We speculated that SRC-2

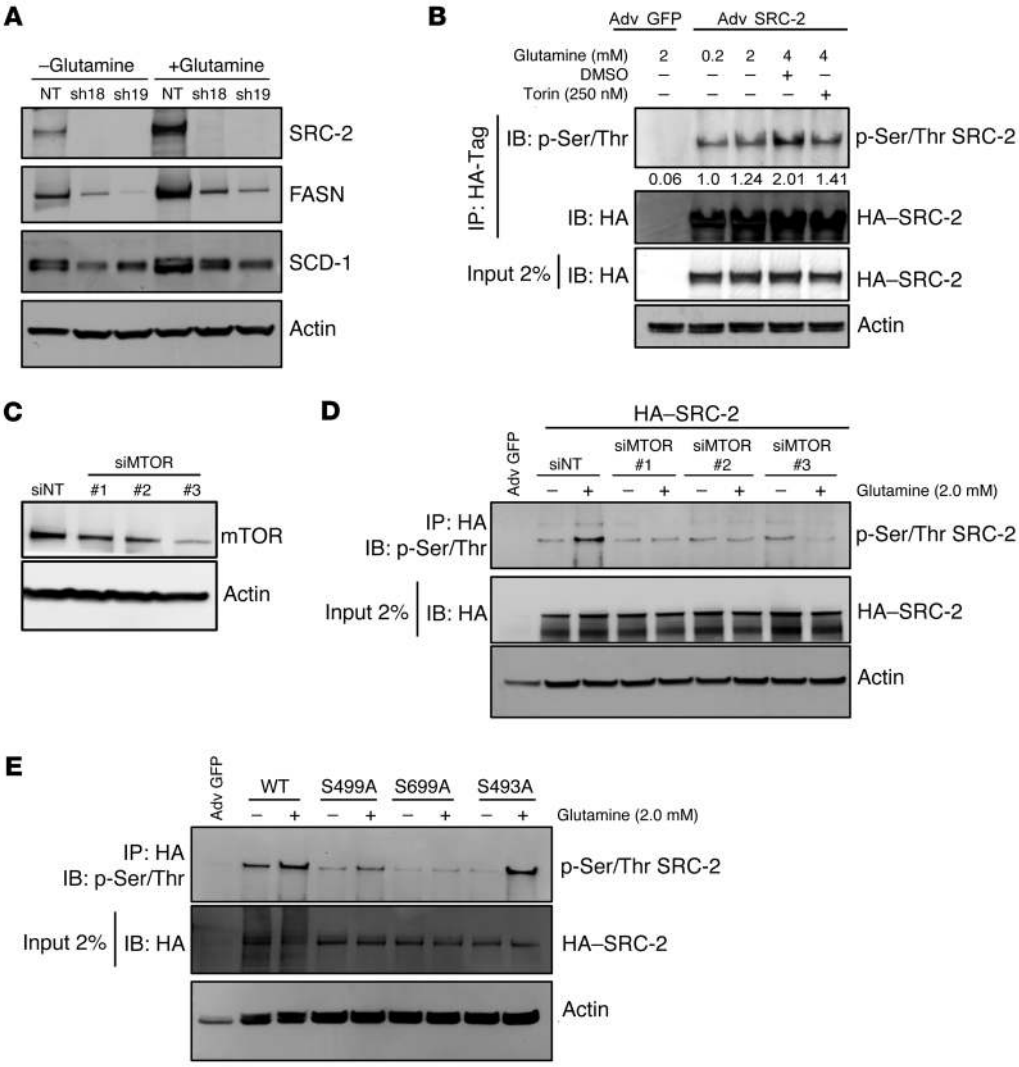

Figure 5. Glutamine stimulation induces mTORC1-dependent phosphorylation of SRC-2. (**A**) Western blot analysis of FASN, SCD, SRC-2, and actin in the stable C4-2 cells shNT, sh18, and sh19 grown with or without glutamine (2 mM). (**B**) Immunoprecipitation of HA–SRC-2 followed by Western immunoblotting to detect the phosphorylation status of SRC-2 using phosphorylated serine/threonine (p-Ser/Thr) antibody. Input lysates were obtained from C4-2 cells expressing GFP adenovirus or SRC-2 adenovirus and subsequently stimulated with increasing concentrations of glutamine (0.2 mM, 2 mM, and 4 mM), followed by treatment with DMSO or the mTORC1 inhibitor torin (250 nM). Actin was used to normalize the input loading control. Semiquantitative levels of phosphorylated SRC-2 were analyzed by densitometry, and relative values (compared with those in lane 2) normalized to actin are indicated numerically under each lane. (**C**) Western blot analysis showing the effect of 3 different siRNAs on mTOR expression. (**D**) C4-2 cells expressing SRC-2 adenovirus were transfected with nontargeting siRNA or 3 different mTOR siRNAs, followed by treatment with or without glutamine (2 mM). HA–SRC-2 was immunoprecipitated followed by Western immunoblotting to detect the phosphorylation status of SRC-2. GFP adenovirus was used as a negative control. (**E**) C4-2 cells expressing HA-tagged WT SRC-2 or the phosphorylation-deficient mutants S499A, S699A, and S493A were stimulated with or without glutamine (2 mM). HA was used to immunoprecipitate WT SRC-2 or mutants, followed by Western immunoblotting to detect the phosphorylation status of SRC-2. Actin was used to normalize the input loading control (HA–SRC-2). Actin was used as a control to normalize the protein loading control, and GFP adenovirus was used as a control virus. The full, uncut gels are shown in the Supplemental Material.

is the genetic cause for reduced expression of ZIP1 in prostate tumors, thus indirectly regulating ACO activity. Indeed, we found that *ZIP1* expression was significantly higher in normal prostate cells compared with that in the majority of the tumor cell lines examined, except DU145 (Supplemental Figure 6B), and forced expression of SRC-2 reduced endogenous *ZIP1* expression (Figure 4D) by directly binding to the proximal promoter region (Figure 4E) and repressing gene transcription (Figure 4F). Supporting this observation, we identified higher levels of *Zip1* expression in SRC-2–KO (*Ncoa2*$^{-/-}$) mouse prostate compared with levels in their WT littermates (Supplemental Figure 6C). To validate whether ZIP1 modulates de novo fatty acid biosynthesis, we measured the mass isotopomer distribution of fatty acids in C4-2 cells ectopically expressing ZIP1. Overexpression of ZIP1 significantly decreased the stearate mass isotopomer distribution from [5-^{13}C]glutamine, indicating that ZIP1-mediated repression of ACO hinders the flow of carbon from glutamine to fatty acids (Figure 4G). These findings imply that SRC-2 stimulates ACO enzymatic activity in prostate cells at least in part by repressing ZIP1 expression to generate citrate for lipogenesis (Supplemental Figure 6D). Collectively, these data demonstrate that SRC-2–mediated use of glutamine carbon via the reductive carboxylation pathway is a metabolic adaptation that prostate cancer cells, but not normal cells, have uniquely acquired to support lipogenesis.

Glutamine uptake stimulates SRC-2 function. Next, we investigated the upstream signaling events that direct SRC-2 to promote glutamine-dependent lipogenesis. Recent studies identified glutamine as a potent signaling molecule (35), especially in a nutrient-stressed environment, as this molecule stimulates nutrient uptake and energy metabolism (36). When we increased glutamine concentrations, we observed an elevation in the expression of 2 SRC-2 target genes, *FASN* and *SCD*, which were subsequently hindered in SRC-2–depleted cells (Figure 5A and Supplemental Figure 7A). Quite unexpectedly, we observed a robust increase in SRC-2 protein levels (Figure 5A), but not mRNA levels (Supplemental Figure 7A), in glutamine-rich cul-

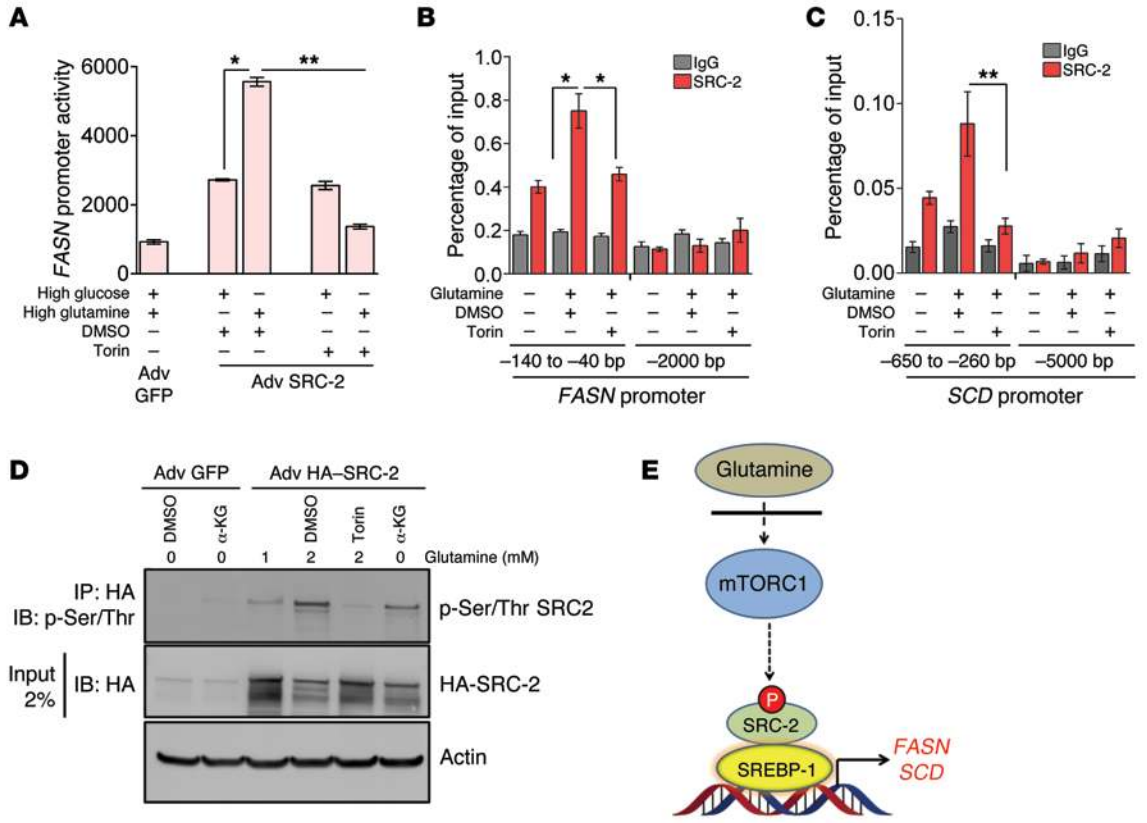

Figure 6. Glutamine stimulation enhances the transcriptional activity of SRC-2. (**A**) PC-3 cells expressing either GFP adenovirus or SRC-2 adenovirus were transfected with an FASN-luciferase construct and stimulated with high glucose (11 mM)/low glutamine (0.2 mM) or high glutamine (2 mM)/low glucose (5 mM) concentrations, followed by treatment with DMSO or torin (250 nM). A luciferase assay was then performed to measure *FASN* promoter activity, and data were normalized to total protein ($n = 4$). (**B** and **C**) ChIP of SRC-2 from C4-2 cells showing the differential recruitment of SRC-2 on the *FASN* and *SCD* promoters upon glutamine stimulation (2 mM) in the presence or absence of torin (250 nM). The amplicons tested are indicated in the figure. IgG antibody was used as a control, and data are presented as the percentage of input chromatin ($n = 3$). (**D**) Immunoprecipitation of HA–SRC-2 followed by Western immunoblotting to detect the phosphorylation status of SRC-2 using phosphorylated serine/threonine antibody. Input lysates were obtained from C4-2 cells expressing GFP adenovirus or SRC-2 adenovirus and subsequently stimulated with increasing concentrations of glutamine (0.2 mM and 2 mM), followed by treatment with DMSO or the mTORC1 inhibitor torin (250 nM). Cell-permeable octyl-α-ketoglutarate was used to rescue the effects of low glutamine levels on SRC-2 phosphorylation. Actin was used to normalize the loading input. The full, uncut gels are shown in the Supplemental Material. (**E**) Schematic depicting the proposed glutamine/mTORC1 signaling pathway, with SRC-2 as the key downstream mediator regulating transcriptional functions that coactivate SREBP-1. Data represent the mean ± SEM. $^*P < 0.05$ and $^{**}P < 0.001$ by Student's *t* test with Holm-Sidak multiple comparisons test.

ture conditions, suggesting a posttranslational regulation of SRC-2 in glutamine-stimulated prostate cancer cells.

Posttranslational modifications such as phosphorylation have the potential to activate and increase protein turnover of the SRC family of coactivators (37), and recent reports have identified PI3K-AKT and mTORC1 as kinases that are potentially activated by nutrient uptake (11, 38). Thus, we examined SRC-2 protein expression in glutamine-stimulated C4-2 cells treated with different kinase inhibitors targeting PI3K-AKT and mTORC1 and compared the effects with those in glucose-stimulated cells. In glutamine-stimulated conditions, SRC-2 protein levels were downregulated by the mTORC1 inhibitor torin compared with the levels detected in DMSO-treated cells (Supplemental Figure 7B), without any appreciable change in SRC-2 messenger expression (Supplemental Figure 7C). However, we did not observe this effect in high-glucose/low-glutamine conditions, and instead, treatment with the PI3K inhibitor wortmannin (WORT) showed some reduction in SRC-2 protein levels (Supplemental Figure 7B). Surprisingly, rapamycin, a well-known inhibitor of mTORC1, failed to mimic the effects of torin, indicating that SRC-2 may be one of the rapamycin-insensitive substrates of mTORC1, as postulated by others (39). Similarly, BEZ-235, a dual inhibitor of PI3K/mTORC1, failed to show any effect on SRC-2 protein stability in either culture condition.

Increasing the concentration of glutamine treatment stimulates mTORC1 kinase activity (35), as indicated in our study by phosphorylation of the mTORC1 substrates S6K1 and 4E-BP1 (Supplemental Figure 7D), and immunoprecipitation of HA-SRC-2 from glutamine-treated C4-2 cells showed a dose-dependent increase in SRC-2 serine/threonine phosphorylation that was subsequently reversed by torin treatment (Figure 5B). To validate that mTORC1 is responsible for phosphorylating SRC-2 upon glutamine stimulation, we induced genetic inhibition of mTORC1 using 3 specific siRNAs (Figure 5C) and observed reduced levels of phosphorylated SRC-2 in C4-2 cells (Figure 5D). Previous proteomic screens to determine mTOR substrates have identified 3 potential sites on SRC-2: S499, S699, and S493 (40, 41). So,

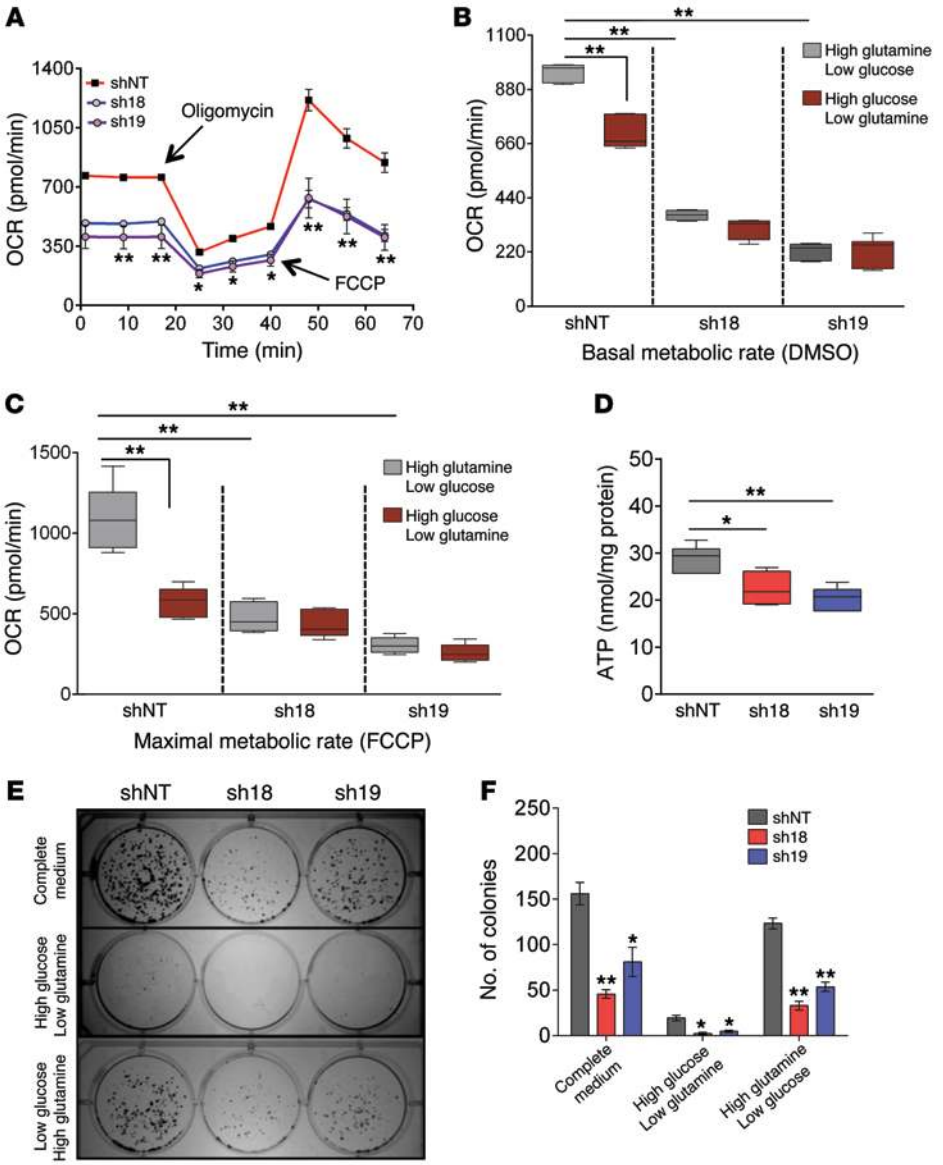

Figure 7. SRC-2 defines the metabolic and energetic program of human prostate cancer cells. (**A**) Real-time measurement of basal and maximal OCRs in the stable C4-2 cells shNT, sh18, and sh19 (n = 3/group). $^*P < 0.05$ and $^{**}P < 0.001$ versus shNT by 2-way ANOVA with Tukey's multiple comparisons test. (**B** and **C**) Basal and maximal OCRs in the stable C4-2 cells shNT, sh18, and sh19 were measured in DMSO control (**B**) or FCCP-treated (**C**) cells cultured in the presence of high glucose (11 mM)/low glutamine (0.2 mM) or low glucose (5 mM)/high glutamine (2 mM) concentrations (n = 3/group). Box and whisker plots indicate the minimum to maximum values (whiskers), 25% and 75% quartiles (boxes), and the median (horizontal lines). $^{**}P < 0.001$ by 2-tailed Student's t test. (**D**) Intracellular ATP levels in the stable C4-2 cells shNT, sh18, and sh19 cultured in complete media (n = 3/group). Box and whisker plot shows the minimum to maximum values (whiskers), 25% and 75% quartiles (boxes), and the median (horizontal lines). $^*P < 0.05$ and $^{**}P < 0.001$ by 1-way ANOVA. (**E**) Clonogenic survival assay showing the number of C4-2 cells stably expressing shNT, sh18, and sh19 clones that survived a 2-week period of nutritional stress. (**F**) Total number of colonies observed in the clonogenic survival assay shown in **E**. Data represent the mean ± SEM. $^*P < 0.05$ and $^{**}P < 0.001$ by Student's t test.

we performed site-directed mutagenesis to generate serine-to-alanine phosphorylation-deficient mutants and found that the S699 site on SRC-2 was primarily phosphorylated by mTORC1 upon glutamine stimulation, whereas S499 showed partial effects (Figure 5E). These data suggest that glutamine stimulation post-translationally modifies SRC-2 by phosphorylation in an mTORC1-dependent manner. Next, we investigated the mechanism by which mTORC1-dependent phosphorylation on SRC-2 enhances SRC-2 protein levels. For this, we performed cycloheximide protein degradation experiments in C4-2 cells cultured in low glutamine (0.2 mM) or high glutamine (2.0 mM) concentrations. Glutamine stimulation significantly increased SRC-2 protein stability and half-life, as determined by cycloheximide time-dependent treatments (Supplemental Figure 8A), but this increased SRC-2 protein stability was completely suppressed by the mTORC1 inhibitor torin (Supplemental Figure 8B). These findings indicate that glutamine-mTORC1–dependent phosphorylation on SRC-2 confers stability to the SRC-2 protein by increasing its half-life, thereby promoting increased levels of SRC-2 protein expression.

Finally, we investigated whether mTORC1 inhibition affects the transcriptional activity of SRC-2. Glutamine signaling induced SRC-2–driven *FASN* promoter activity (Figure 6A) as well as enhanced recruitment of SRC-2 to the *FASN* and *SCD* promoters (Figure 6, B and C), and this glutamine-dependent SRC-2 activity was significantly blocked by torin (Figure 6, A–C). Since glutamine has been reported to facilitate mTORC1 activation in a RAG-dependent manner via α-ketoglutarate (35), we used the cell-permeable α-ketoglutarate analog octyl-α-ketoglutarate to reverse the low glutamine conditions in SRC-2 phosphorylation. As shown in Figure 6D, glutamine stimulation increased SRC-2 phosphorylation, whereas torin treatment reduced phosphorylation of SRC-2. In contrast, the α-ketoglutarate analog octyl-α-ketoglutarate partially reversed the low glutamine levels in the phosphorylation of SRC-2, indicating that glutamine-dependent mTORC1 activation stimulates phosphorylation of its downstream target SRC-2 in a RAG-dependent fashion. In addition, the mTORC1 inhibitor torin also recapitulated the reduced lipid levels, as observed under SRC-2–ablated conditions (Supplemental Figure 9, A–E). Taken

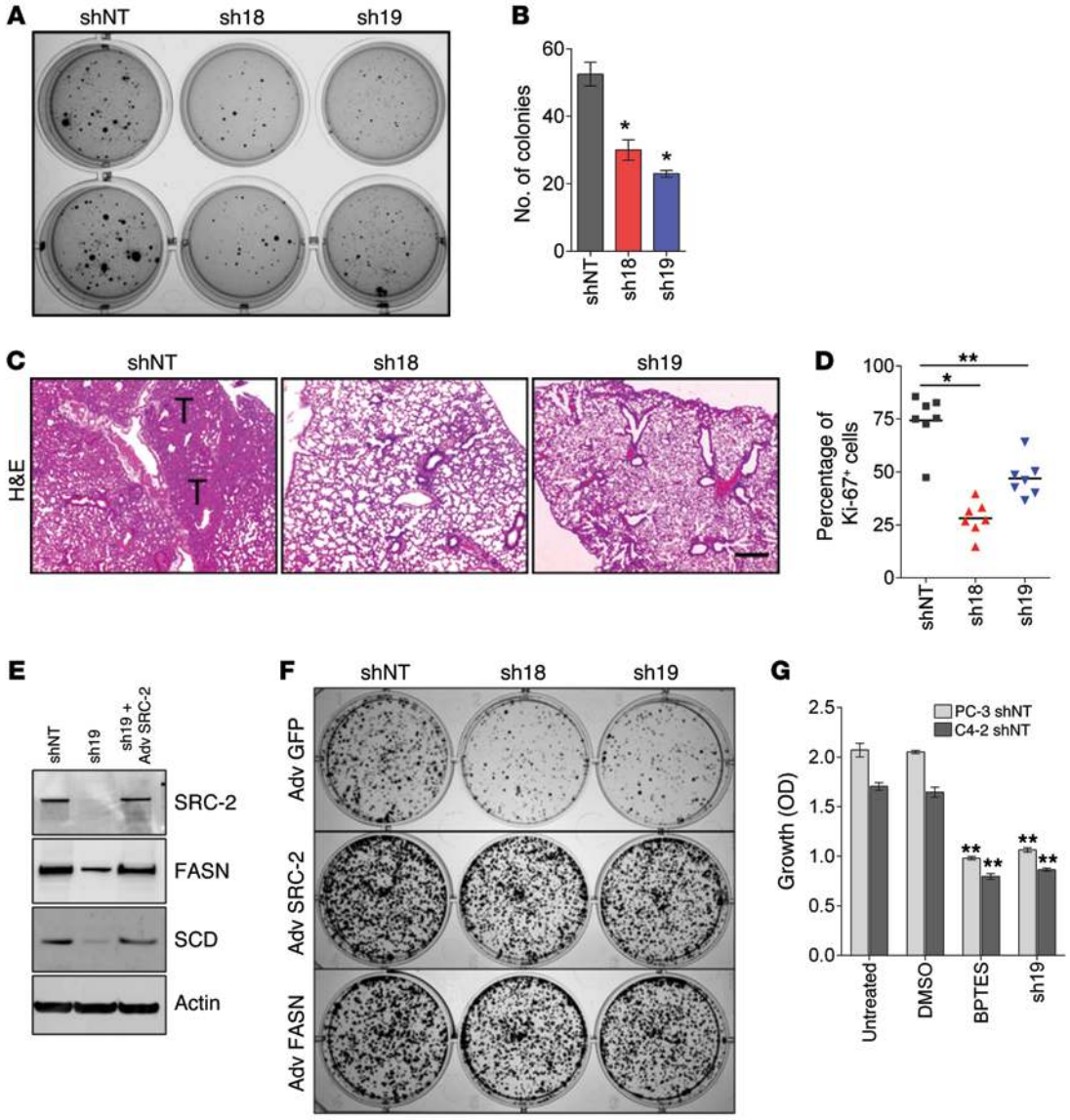

Figure 8. SRC-2 is essential for prostate cancer cell survival. (**A**) Representative images depicting the growth of the stable C4-2 cells shNT, sh18, and sh19 in soft agar assay 2 weeks after plating. (**B**) Quantification of the total number of stable C4-2 cell colonies that survived after 2 weeks. *P <0.05 by 1-way ANOVA. (**C**) H&E-stained sections of mouse lungs from experimental lung metastasis assay. Nude mice were injected via the tail vein with PC-3 cells stably expressing shNT, sh18, and sh19 (n = 7), and growth and survival of the cells in mouse lungs were analyzed after 5 weeks. T, tumor. Scale bar: 100 μm. (**D**) Quantification of Ki67-stained cells (antibody epitope reacts with human Ki67 protein) in mouse lung sections from shNT-, sh18-, and sh19-injected animals. *P < 0.05 and **P < 0.001 by 2-tailed Student's t test. Refer also to Supplemental Figure 11C. (**E**) Western blot analysis showing expression levels of SRC-2, FASN, SCD, and actin in the stable C4-2 cells shNT and sh19, and reexpression of SRC-2 in sh19 cells infected with SRC-2 adenovirus. Actin was normalized to the protein loading control. The full, uncut gels are shown in the Supplemental Material. (**F**) Clonogenic survival assay in the stable PC-3 cells shNT, sh18, and sh19 expressing GFP adenovirus, SRC-2 adenovirus, or FASN adenovirus to rescue the defective survival phenotype in SRC-2–depleted cells. (**G**) Relative growth of C4-2 and PC-3 cells stably expressing shNT that were either untreated or treated with DMSO or BPTES (1 μM) for 4 days. sh19 cells were used to monitor the effect of SRC-2 knockdown (n = 6/group). Data represent the mean ± SEM. *P < 0.05 compared with DMSO and **P < 0.001 by 2-way ANOVA with Tukey's multiple comparisons test.

together, these data demonstrate that glutamine uptake by tumor cells activates SRC-2 in an mTORC1-dependent manner (Figure 6E), which in turn, transcriptionally regulates the expression of FASN and SCD, thus promoting lipogenesis.

SRC-2 defines the bioenergetics of prostate cancer cells. To investigate whether SRC-2 expression defines the metabolic state of tumor cells, we analyzed the bioenergetic parameters of prostate cancer cells upon perturbation of SRC-2. SRC-2–ablated C4-2 and PC-3 cells showed a significantly reduced basal metabolic rate (refer to the 0- to 20-minute time frame in the figures) compared with that of control shNT cells (Figure 7A and Supplemental Figure 10A). While oligomycin treatment decreased oxygen consumption (refer to the 25- to 40-minute time frame), addition of the uncoupler carbonyl cyanide 4-(trifluoromethoxy)phenylhydrazone (FCCP) dramatically enhanced the oxygen consumption rate (OCR), indicating the maximal respiratory capacity (refer to the 45- to 65-minute time

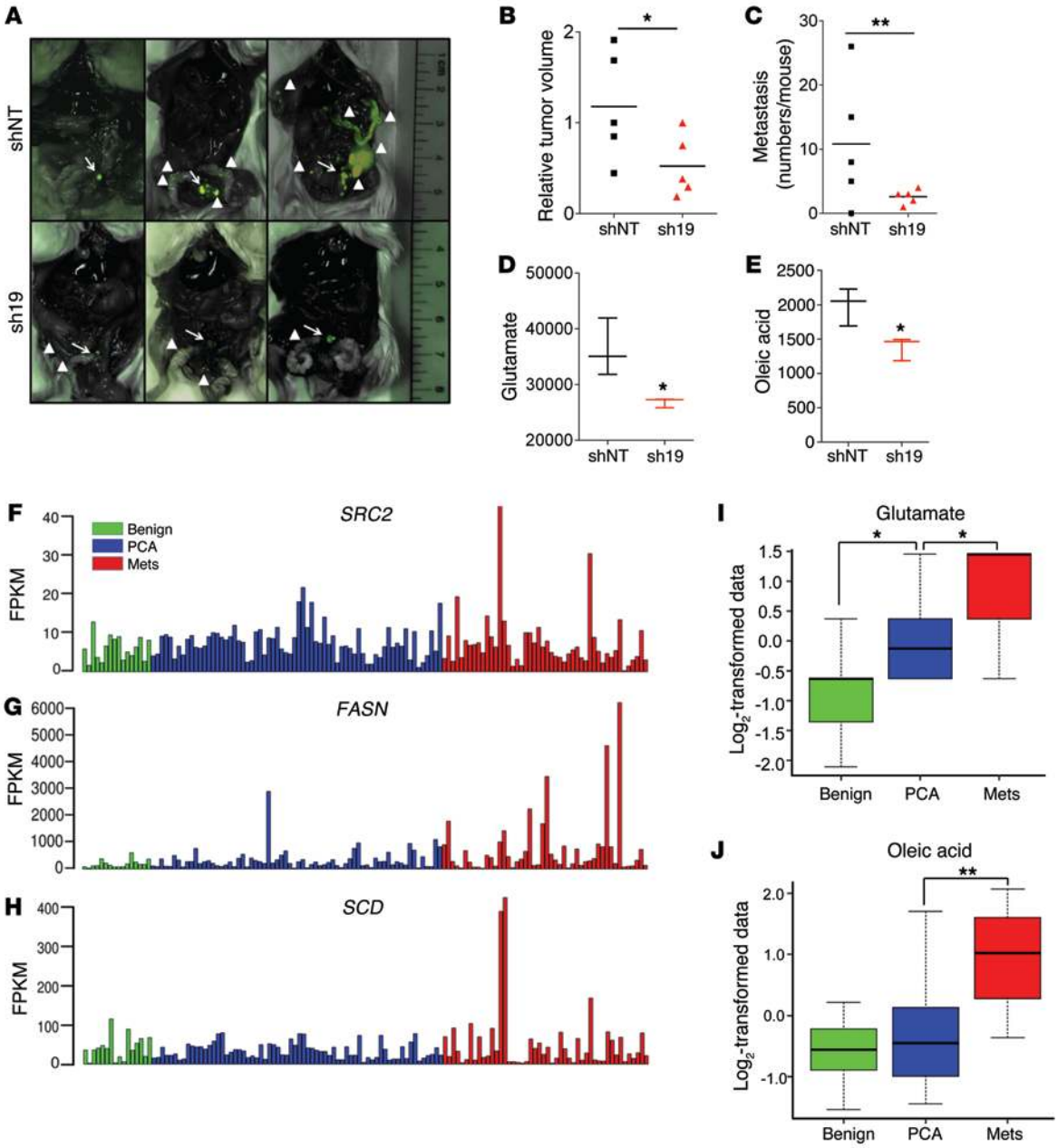

Figure 9. SRC-2 promotes prostate cancer metastasis. (**A**) PC-3 cells stably expressing shNT and sh19 (n = 5) were orthotopically implanted into the left ventral prostate lobe of SCID mice and imaged 8 weeks after surgery using a UVP Biospectrum imager. Arrows indicate the primary tumors, and arrowheads show the location of metastatic spreading. (**B** and **C**) Each primary tumor was measured using slide calipers, and relative tumor volumes (**B**) and metastases (**C**) were plotted for each mouse (horizontal line represents the mean). (**D** and **E**) Targeted MS analysis of xenograft tumor extracts from PC-3 shNT and sh19 cells depicted in **A** showing the relative levels of glutamate and oleic acids. (**F**–**H**) Fragments per kilobase of exon per million fragments mapped (FPKM) values of *SRC2*, *FASN*, and *SCD* from a cohort of benign adjacent (n = 16), organ-confined prostate cancer (n = 68) and metastatic prostate cancer (n = 48). (**I** and **J**) Log_2-transformed data depicting the levels of glutamate and oleic acid from benign adjacent prostate (n = 16), clinically localized prostate cancer (n = 12, PCA), and metastatic prostate cancer (n = 14) tissues (46). This cohort is a subset of the RNA-seq cohort shown in **F**–**H**. *$P < 0.05$ and **$P < 0.001$ by Student's t test. For metabolomic analyses, we calculated a permutation-based P value (10,000 permutations of sample labels) to define the significance of metabolites in different categories (45).The data were plotted as a box plot in R language and show the 5% and 95% quantiles (whiskers), 25% and 75% quartiles (box), and the median (horizontal line). *$q < 0.05$ and **$q < 0.001$ by 2-sided Student's t test, with an FDR-corrected P value of less than 0.05 considered significant.

frame) in prostate cancer cells (Figure 7A and Supplemental Figure 10A). However, SRC-2–depleted cells showed a significantly reduced maximal metabolic rate compared with that of control (shNT) cells, demonstrating its importance in regulating the bioenergetics of prostate cancer cells (Figure 7A and Supplemental Figure 10A).

We next measured the metabolic rate of tumor cells cultured in different nutrient conditions. Prostate cancer cells (shNT) exposed to high glutamine/low glucose levels exhibited both higher basal (Figure 7B and Supplemental Figure 10B) and maximal metabolic rates (Figure 7C and Supplemental Figure 10C)

compared with those in cells exposed to high glucose/low glutamine levels, indicating the importance of glutamine metabolism in the maintenance of a robust energetics program. In contrast, SRC-2–ablated cells exhibited significantly lower basal (Figure 7B and Supplemental Figure 10B) and maximal metabolic rates (Figure 7C and Supplemental Figure 10C), with a reduced proliferative rate, compared with the rates observed in control cells (Supplemental Figure 10, D–F). We also observed that the maximal metabolic rate (Figure 7C) and proliferative capacity (Supplemental Figure 10, E and F) of SRC-2–depleted cells exposed to high glutamine/low glucose concentrations were similar to those seen in control cells cultured in high glucose/low glutamine concentrations, suggesting that loss of SRC-2 mimics a glutamine-deprived metabolic state. As expected, genetic inhibition of SRC-2 in prostate cancer cells led to a significantly reduced intracellular ATP pool, which exemplifies a metabolically defective cellular state (Figure 7D). Colony-formation assays mirrored these effects, as SRC-2–depleted C4-2 and PC-3 cells showed poor survival (Figure 7, E and F, and Supplemental Figure 10, G and H). Taken together, these findings confirm that SRC-2 coordinates the metabolic functioning of tumor cells and promotes prostate cancer cell survival, even under conditions of nutrient stress.

SRC-2 is a survival factor for prostate cancer metastasis. Tumor cell survival and proliferation are the major hallmarks of the metastatic dissemination of cancer cells to distant sites (42). Given the importance of SRC-2 as the prime coordinator of energy metabolism, which balances growth and survival (43), and its increased expression in metastatic prostate cancer patients (18), we investigated the role of SRC-2 in promoting prostate cancer metastasis. Anchorage-independent growth of tumor cells is a crucial step in the acquisition of malignancy, and silencing of SRC-2 significantly reduced the clonal growth of both C4-2 and PC-3 cells in soft agar (Figure 8, A and B, and Supplemental Figure 11, A and B). To determine whether SRC-2 expression promotes in vivo growth and survival of prostate cancer cells during the process of metastatic dissemination, we took advantage of a mouse model of experimental lung metastasis. SRC-2–ablated PC3 cells (sh18 and sh19) injected via the tail vein into nude mice showed significantly reduced colonization and growth of the disseminated tumor cells in lungs 5 weeks after injection compared with what was observed in control PC3 cells (shNT). H&E-stained images clearly indicated reduced growth of SRC-2–ablated metastatic prostate tumor cells in lung parenchyma (Figure 8C), with a reduced proliferative index, as evidenced by Ki67 staining (Figure 8D and Supplemental Figure 11C).

Since loss of SRC-2 simulates a glutamine-deprived metabolic state with reduced growth and poor survival, we investigated whether reconstitution of SRC-2 (Figure 8E and Supplemental Figure 11D) or FASN expression in SRC-2–knockdown cells could rescue the phenotype. While forced overexpression of SRC-2 enhanced PC-3 (Figure 8F and Supplemental Figure 11E) and C4-2 growth and survival (Supplemental Figure 11F and Supplemental Figure 12, A and B), reexpression of SRC-2 or its target gene *FASN* in SRC-2–depleted PC-3 cells rescued the survival defects (Figure 8F and Supplemental Figure 11E), whereas partial recovery was achieved in C4-2 cells (Supplemental Figure 11F and Supplemental Figure 12, A and B). Reconstitution of SRC-2 also restored expression of its transcriptional targets *FASN* and *SCD* (Figure 8E) as well as total cellular palmitate levels (Supplemental Figure 12C), confirming that SRC-2 is a prime mediator of the lipogenic program in prostate tumorigenesis. In addition, knockdown of the SRC-2 target gene *SCD* (Supplemental Figure 12D) or overexpression of ZIP1 also mimicked the growth the defective phenotypes (Supplemental Figure 12, E and F) observed in SRC-2–silenced tumor cells.

Next, we exploited the opportunity to target the glutamine metabolic pathway in prostate cancer cells by using BPTES, a specific inhibitor of the glutaminase enzyme GLS1 (44). Treatment with BPTES (1 μM) rapidly blocks the utilization of glutamine in cells (44, 45), and we observed a robust decrease in prostate cancer cell growth compared with that seen with DMSO treatment (Figure 8G). SRC-2 depletion also attenuated the growth of C4-2 and PC-3 cells in a manner similar to that seen in BPTES-treated cells (1 μM); however, at higher doses, the effect of BPTES on cell growth was stronger than that achieved with SRC-2 ablation (data not shown). These findings suggest that targeting the SRC-2 or glutamine metabolic pathway may be beneficial for prostate cancer therapy.

Finally, to confirm that SRC-2 inhibition blocks prostate tumor growth and metastasis, we surgically implanted SRC-2–depleted PC-3 cells (sh19) orthotopically into the mouse prostate and compared primary tumor growth and metastasis with that in the control cells (shNT) 8 weeks after surgery. While mice harboring transplanted shNT PC-3 cells showed robust growth of primary prostate tumors (Figure 9, A and B, and Supplemental Figure 13, A–C) and large numbers of metastatic lesions (Figure 9, A and C, and Supplemental Figure 13A), SRC-2–depleted PC-3 cells developed smaller primary tumors (Figure 9, A and B) and had a dramatically reduced number of metastatic lesions (Figure 9, A and C). Gene expression profiling confirmed significantly lower levels of *FASN* and *SCD* in SRC-2–depleted orthotopic tumors compared with those in shNT PC-3 tumors (Supplemental Figure 13B). Next, we profiled the levels of key metabolites in the mouse orthotopic prostate tumors using MS, which revealed significantly reduced amounts of glutamate (Figure 9D) and fatty acids, such as oleic acid (Figure 9E) and palmitic acid, and low levels of palmitoleic acid in SRC-2–ablated tumors (Supplemental Figure 13D). These findings demonstrate that SRC-2–driven metabolic reprogramming is a critical determinant of prostate cancer cell survival, and this mechanism may select variant clones for aggressive metastasis. Our findings substantiate the dominant role of SRC-2 in prostate cancer growth and metastasis and suggest that inhibition of SRC-2 may be beneficial for treating metastatic prostate cancer.

In order to gain clinical insights, expression levels of *SRC2*, *FASN*, and *SCD* were examined in a patient-derived RNA-seq dataset containing tissue samples ($n = 132$) collected from benign adjacent ($n = 16$), organ-confined prostate cancer ($n = 68$) and metastatic prostate cancer ($n = 48$) tissues. Importantly, we observed enhanced expression of *SRC2* in prostate cancer patients, particularly in those with metastases (Figure 9F), with a concomitant increase in the expression of its transcriptional targets *FASN* and *SCD* (Figure 9, G and H). In the context of these findings, we reanalyzed our previously published metabolomic profiling dataset (46), which was a subset of the larger RNA-seq cohort described above. The metabolomic dataset contained tissues from benign adjacent prostate ($n = 16$), organ-confined prostate cancer ($n = 12$), and metastatic prostate cancer ($n = 14$). We found that glutamate

levels were significantly increased with disease progression from benign to prostate cancer to metastatic prostate cancer (Figure 9I), while a decreasing trend was noted for glucose levels (Supplemental Figure 13E). Fatty acids such as oleic acid (Figure 9J) and palmitoleic acid (Supplemental Figure 13F), on the other hand, were increased in metastatic prostate cancer. These data support our findings that the glutamine-dependent lipogenic program is enhanced in metastatic prostate tumors and that overexpressed SRC-2 is one of the prime regulators of this metabolic reprogramming. These clinical observations substantiate our findings that elevated levels of SRC-2 promote prostate cancer metastasis by imparting metabolic advantages to the tumor cells, thus licensing them for uncontrolled growth and metastasis.

Discussion

Over the past decade, advances in cancer metabolic research have broadened our understanding of the various metabolic alterations prevalent in tumor cells that can support the anabolic requirements of proliferating cells. Despite this knowledge, the higher-order regulatory networks and genetic factors that govern these perturbed metabolic pathways are incompletely understood. Here, we uncover the role of the oncogenic transcriptional coregulator SRC-2 as an underlying metabolic coordinator facilitating growth, survival, and eventually metastasis of prostate tumor cells. We provide evidence that SRC-2 expression defines a metabolically active cellular state by reprogramming cellular metabolism to utilize glutamine for fatty acid biosynthesis. This process supplements the tumor cells with added bioenergetic and biomass proliferative advantages so that anabolic processes are not compromised. Tumor cells encounter a variety of environmental challenges during the process of metastasis, and for successful survival and growth outside the host tissue, an autonomous and highly efficient metabolic strategy providing a constant supply of energy and biosynthetic macromolecules is required. We propose that increased expression of SRC-2 in prostate tumors reinforces these metabolic advantages and that these advantages foster cell survival and homing during metastatic spreading.

Our findings show that SRC-2 promotes de novo fatty acid biosynthesis in prostate cancer cells by 2 distinct but interrelated processes regulating both substrate availability and rate-limiting enzymes. We provide evidence that SRC-2 facilitates synthesis of the lipid precursor molecule citrate from glutamine by reversal of canonical TCA cycle reactions through reductive carboxylation. Although, this reductive carboxylation pathway has been considered to be less efficient in mammalian cells, recent reports have indicated that cancer cells can efficiently utilize this pathway for lipid synthesis (5, 47). Mechanistically, SRC-2 promotes reductive carboxylation by activating the ACO enzyme via transcriptional repression of the zinc transporter ZIP1, whose expression is found to be significantly reduced in prostate cancer patients (34). Since zinc is an allosteric inhibitor of ACO enzyme activity (33), prostate cancer cells have uniquely acquired this ability to block the entry of zinc by SRC-2–mediated downregulation of its transporter. In addition, SRC-2 coactivates the SREBP-1 transcription factor to enhance expression of the key enzymes of de novo lipogenesis, FASN and SCD, independently of the AR, clearly substantiating that SRC-2 does not act wholly via the AR. Thus, dynamic regulation by overexpressed SRC-2 in prostate tumor cells, both as a coactivator and corepressor, fine-tunes metabolic rewiring to favor the lipogenic program.

Recent findings have identified mTORC1 as an integral member of the glutamine-signaling pathway, regulating glutamine anaplerosis to sustain tumor cell growth and proliferation (48). Our findings now broaden this understanding by providing evidence that glutamine/mTORC1 signaling stimulates and recruits SRC-2 to coordinate transcriptional changes to activate metabolic genes. Thus, our study now identifies SRC-2 as a crucial downstream mediator of the glutamine/mTORC1 signaling pathway that promotes de novo lipogenesis in prostate cancer cells.

Traditionally, altered metabolism in cancer cells is viewed as an indirect phenomenon secondary to growth signals (42), but recent evidence supports an alternative concept, which advocates that the primary functions of activated oncogenes and tumor suppressors may be to reprogram tumor metabolism (3). In line with this new concept, our findings suggest that the oncogenic functions of SRC-2 are primarily attributed to its ability to maintain increased fatty acid biosynthesis and energy homeostasis, thereby enhancing proliferative signals for cell growth and survival by evading cell death and growth-suppression checkpoints. Supporting this notion, previous findings have identified the oncogenic potential and growth-promoting functions of *FASN* and *SCD*, 2 of the SRC-2 downstream target genes identified in this study (8, 49). Thus, it is reasonable to postulate that coactivator-dependent transcriptional reprogramming plays a major role in resetting the tumor metabolic pathways to support uncontrolled growth and survival. In addition, our study identified that prostate tumor cells are addicted to glutamine metabolism under conditions of nutrient stress and during the progression of the disease from localized to metastatic cancer, and inhibition of either SRC-2 or the glutamine metabolic pathway can significantly reduce tumor cell growth and metastasis. In summary, we believe that our results provide novel insights that could lead to the development of anticancer therapeutic strategies to target cellular metabolism in prostate cancers.

Methods

Cell culture

LNCaP, C4-2, and PC-3 cells were cultured in RPMI (Invitrogen) supplemented with 10% FBS (Invitrogen) and penicillin-streptomycin (PS) (Invitrogen). The C4-2 cell line was a gift of Nancy Weigel (Baylor College of Medicine, Houston, Texas, USA). HeLa cells were cultured in DMEM (Invitrogen) with 10% FBS and 1% PS. For nutrient-stressed experiments, the following media compositions were used: high glucose/low glutamine concentrations consisting of RPMI[-] glutamine (21870; Invitrogen) supplemented with 0.2 mM L-glutamine (Invitrogen) at a final concentration of D-glucose (11 mM), 10% dialyzed FBS, and 1% PS. Low glucose/high glutamine concentrations consisting of RPMI[-]glucose (11879; Invitrogen) at a final L-glutamine concentration of 2.0 mM, supplemented with 5 mM D-glucose, 10% dialyzed FBS, and 1% PS.

Reagents and plasmids

Kinase inhibitors were obtained from the following sources: rapamycin (Calbiochem); torin 1 (Tocris); BEZ235 (Selleck Chemicals); WORT (Sigma-Aldrich); octyl-α-ketoglutarate (Cayman Chemical); and BPTES

inhibitor (gift of Takashi Tsukamoto, Johns Hopkins University, Baltimore, Maryland, USA). The following antibodies were used: SRC-2 (BD Biosciences and Bethyl Laboratories); SCD (Abcam); FASN, mTORC1 sampler kit, and HA-Tag (Cell Signaling Technology); and phosphoserine/threonine (BD Biosciences). The following plasmids were used: pCR3.1-SRC-2 and pcDNA3.1-FLAG-SREBP-1a (Addgene); pGL3-ZIP1 and FASN luciferase (Addgene); and SCD luciferase (SwitchGear Genomics). The pGL3-hZIP1 (–246/+82) construct was a gift of Peter Makhov (Fox Chase Cancer Center, Philadelphia, Pennsylvania, USA) (50).

Animals

All animal experiments were performed in accordance with the Animal Care Research Committee at Baylor College of Medicine. The generation of the SRC-2–KO (*Ncoa2*$^{-/-}$) mice has been described previously (51), and age-matched male littermate mice were used. For tumor studies, 6- to 7-week-old male athymic nude mice (Harlan Laboratories) were used for experimental lung metastasis assays and 6- to 7-week-old male Fox Chase SCID mice (Charles River Laboratories) for prostate orthotopic xenograft experiments.

Lentivirus-mediated generation of cells with knockdown of SRC-2

Stable cells with decreased expression of SRC-2 were generated by lentivirus-mediated shRNA expression. The pGIPZ vector expressing shRNA sequences targeting SRC-2 (2 clones: 186064 and 199063) or nontargeting controls (control: shNT) were obtained from OpenBiosystems, and viruses were generated at the Cell-Based Assay Screening Service of the Baylor College of Medicine (CBASS-BCM) Core Facility. Polyclonal pooled populations of stable cells were selected in the presence of puromycin (1 μg/ml) for more than 3 passages before initiating any functional or tracer experiments.

Luciferase assay

Luciferase assays were performed using the Luciferase Reporter Assay (Promega) and a Berthold 96-well plate reader. Luciferase values were normalized to the total protein level.

ChIP

ChIP assays were performed using an EZ ChIP kit (EMD Millipore) with some modification. Briefly, stable C4-2 cells were grown in 15-cm dishes until 80% confluence and stimulated with glutamine with or without torin (250 nM), followed by chromatin shearing and qPCR.

Metabolomic profiling

Reagents and internal standards. HPLC-grade acetonitrile (ACN), methanol, and water were purchased from Burdick & Jackson. MS-grade formic acid and internal standards, namely, [15N]$_2$tryptophan, and [15N]anthranilic acid were purchased from Sigma-Aldrich. The calibration solution containing multiple calibrants in ACN/trifluroacetic acid/water was purchased from Agilent Technologies. Metabolomics analyses of all samples were performed using the protocol described previously. The raw data (liquid chromatography–MS [LC-MS] output) were normalized using internal standards (52).

LC-MS

The chromatographic separation of metabolites was performed using either reverse-phase separation or normal-phase separation online with a QQQ mass spectrometer (Agilent Technologies).

Separation of TCA metabolites. Normal-phase chromatographic separation was also used for targeted identification of metabolites (52). This procedure involved the use of solvents containing water (solvent A), with solvent A modified by the addition of 5 mM ammonium acetate (pH 9.9) and 100% ACN (solvent B). The binary pump flow rate was 0.2 ml/minute, with a gradient spanning 80% B to 2% B for 20 minutes, followed by 2% B to 80% B for 5 minutes, which was then followed by 80% B for 13 minutes. The flow rate was gradually increased during the separation from 0.2 ml/minute (0–20 minutes), to 0.3 ml/minute (20.1–25 minutes), to 0.35 ml/minute (25–30 minutes), to 0.4 ml/minute (30–37.99 minutes), and was finally set at 0.2 ml/minute (5 minutes). Metabolites were separated on a Luna Amino (NH2) column (4 μm, 100A 2.1 × 150 mm; Phenominex), which was maintained in a temperature-controlled chamber (37°C). All the columns used in this study were washed and reconditioned after every 50 injections.

Separation of fatty acids (palmitoleic acid and oleic acid). Targeting the metabolites, reverse-phase chromatographic separation was performed to identify metabolites. Solvents containing water (solvent A) were used for this separation, with solvent A modified by the addition of 10 mM ammonium acetate (pH 8) and 100% methanol (solvent B). The binary pump flow rate was 0.2 ml/minute, with a gradient spanning 40% B to 50% B for 8 minutes, followed by 50% B to 67% B for 5 minutes, a hold of 67% B for 9 minutes, followed by 67% B to 80% B for 1 minute, followed by 80% B to 100% B for 4 minutes, and a hold of 100% B for 5 minutes. Metabolites were separated on a Phenyl Hexyl column (3 μm, 100A 2.1 × 150 mm; Phenominex) that was maintained in a temperature-controlled chamber (37°C). All the columns used in this study were washed and reconditioned after every 50 injections.

Sample preparation for MS-based examination of metabolome from orthotopic mouse tumors

Orthotopic mouse tissues were stored at –140°C in liquid nitrogen until analysis. For metabolome extraction, 10 mg of tissue was homogenized in a 1:4 ice-cold water/methanol mixture containing [15N]$_2$tryptophan. This was followed by the sequential addition of ice-cold chloroform and water at a 3:1 ratio and separation of the organic (methanol and chloroform) and aqueous solvents (water/methanol/chloroform/water at a ratio of 1:4:3:1). The aqueous extract was deproteinized using a 3-kDa molecular filter (Amicon Ultracel 3-kDa Membrane; EMD Millipore), and the filtrates containing metabolites were dried under vacuum (EZ-2 Plus; Genevac). Prior to MS, the dried extract was resuspended in an identical volume of injection solvent composed of the appropriate mobile phase and subjected to LC-MS.

Separation of metabolites. Reverse-phase chromatographic separation was performed for the targeted identification of metabolites. For this, we used a solvent containing water (solvent A); solvent A was modified by the addition of 10 mM ammonium acetate and 100% methanol (MeOH) to form solvent B. Gradient: 40% B to 100% B for 23 minutes. Flow rate: 0.2 ml/minute. Metabolites were separated on a Luna Phenyl Hexyl column (3 μm, 2 × 150 mm) that was maintained in a temperature-controlled chamber (40°C).

Isotope labeling and profiling by targeted MS

Nutrients labeled with ^{13}C were purchased from Cambridge Isotope Laboratories. C4-2 cells were grown in 6-well plates in regular media until 80% confluence, followed by overnight starvation and then addition of 2.0 mM L[U-$^{13}C_5$]glutamine, [1-^{13}C]glutamine, or [5-^{13}C]

glutamine supplemented with RPMI[-]glutamine with 10% dialyzed FBS and 1% PS, or addition of 11 mM D[U-$^{13}C_6$]glucose supplemented with RPMI[-]glucose, 10% dialyzed FBS, and 1% PS. Culture medium was collected, cells were washed with PBS, and equal numbers of cells from each treatment were snap-frozen with liquid nitrogen. Cells were scraped into a 0.5-ml mixture of 1:1 water/methanol, sonicated for 1 minute (two 30-second pulses), and then mixed with 450 μl ice-cold chloroform. The resulting homogenate was then mixed with 150 μl ice-cold water and vortexed again for 2 minutes. The homogenate was incubated at –20°C for 20 minutes and centrifuged at 4°C for 10 minutes to partition the aqueous and organic layers. The aqueous and organic layers were combined and dried at 37°C for 45 minutes in an automatic Environmental Speed Vac system (Thermo Fisher Scientific). The extract was reconstituted in a 500-μl solution of ice-cold methanol/water (1:1) and filtered through a 3-kDa molecular filter (Amicon Ultracel 3-kDa Membrane) at 4°C for 90 minutes to remove proteins. The filtrate was dried at 37°C for 45 minutes in a speed vacuum and stored at –80°C until MS analysis. Prior to MS analysis, the dried extract was resuspended in a 50-μl solution of methanol/water (1:1) containing 0.1% formic acid and then analyzed using multiple reaction monitoring (MRM). Ten microliters was injected and analyzed using a 6490 QQQ triple quadrupole mass spectrometer (Agilent Technologies) coupled to a 1290 Series HPLC system via selected reaction monitoring (SRM). Metabolites were targeted in both positive and negative ion modes: the electrospray source ionization (ESI) voltage was +4,000 V in positive ion mode and –3,500 V in negative ion mode. Approximately 9 to 12 data points were acquired per detected metabolite. To target the TCA flux, the samples were delivered to the mass spectrometer via normal-phase chromatography using a Luna Amino column (4 μm, 100A 2.1 × 150 mm). To target the fatty acid flux, the samples were delivered to the mass spectrometer via reverse-phase chromatography using a Phenyl Hexyl column (3 μm, 100A 2.1 × 150 mm). For ^{13}C-labeled experiments, SRM was performed for expected ^{13}C incorporation in various forms for targeted LC-MS/MS. Mass isotopomer distribution (MID) was calculated using the formula: [fractional incorporation = (^{13}C/^{13}C + ^{12}C) × 100] and corrected for natural abundance. The change in reductive carboxylation flux was calculated by comparing the MIDs of TCA metabolites from [1-^{13}C]glutamine– or [5-^{13}C]glutamine–labeled cells. The fractional contribution of lipogenic acetyl CoA was determined by regression modeling of palmitate MIDs from [5-^{13}C] glutamine–labeled cells.

Enzymatic activity

IDH (MAK062; Sigma-Aldrich), CS (CS0720; Sigma-Aldrich), and ACO (MAK051; Sigma-Aldrich) enzymatic activity was measured using the kits according to the manufacturer's protocol. Briefly, cells were seeded in 15-cm dishes until 80% confluence. Cells were lysed in ice-cold conditions using the lysis buffer provided in the kit supplemented with protease and phosphatase inhibitor cocktail (EMD Millipore). Equal amounts of protein were used for the enzymatic activity assay.

Metabolomic data analysis

Normalized data were obtained from Sreekumar A et al. (46). We performed a permutation-based *P* value (10,000 permutations of sample labels) to define the significance of metabolites in different categories. The data were further plotted using box plotting in R language.

GSEA

GSEA was carried out using the GSEA software package (53). The NES and adjusted *q* values were computed using the GSEA method, based on 1,000 random permutations of the ranked genes. The data were deposited in the NCBI's Gene Expression Omnibus database (GEO GSE63539).

Statistics

Unless otherwise indicated, all results represent the mean ± SEM, and statistical comparisons between different groups were performed using the 2-tailed Student's *t* test or 2-way ANOVA with Tukey's multiple comparisons corrections. For all statistical analyses, differences of $P \leq 0.05$ were considered statistically significant, and experiments were repeated at least 3 times. GraphPad Prism software version 4.0/6.0 (GraphPad Software) was used for data analysis.

Study approval

All animal experiments were approved by the Animal Center for Comparative Medicine at Baylor College of Medicine (BCM). The prostate tissue samples used for metabolomics and RNA-seq analysis were previously reported, and data analyses were performed with the approval of the IRB of BCM.

Acknowledgments

We thank the following colleagues and core facilities at BCM for their help with the study: Nancy Weigel (helpful discussion); Bokai Zhu and Bin He (ChIP-seq analysis); Bian Ka and Vasanta Putluri (technical assistance); Pradip Saha (seahorse experiments); the Tissue Culture Core Facility, CBASS, and the Pathology and Tissue Core Facility. The Mouse Metabolic Core (MMC) and the Diabetes Research Center at BCM were supported by National Institute of Diabetes and Digestive and Kidney Diseases (NIDDK), NIH grant P30 DK079638. This work was supported by a Challenge Award from the Prostate Cancer Foundation (to B.W. O'Malley); the NIDDK, NIH (5P01DK059820, to B.W. O'Malley); the Cancer Prevention Research Institute of Texas (CPRIT) (RP100348, to B.W. O'Malley); a Center for the Advancement of Science in Space (CASIS) Integrated Omics Award (to B.W. O'Malley); CPRIT Multi-Investigator Research Awards (CPRIT-MIRA) (RP101251-P02, to B.W. O'Malley, and RPN120092 and 1R01CA133458, to A. Sreekumar); and the National Cancer Institute (NCI), NIH (1U01CA167234 to A. Sreekumar).

Address correspondence to: Bert W. O'Malley, Department of Molecular and Cellular Biology, Baylor College of Medicine, One Baylor Plaza, Houston, Texas 77030, USA. Phone: 713.798.6205; E-mail: berto@bcm.edu.

1. Vander Heiden MG, Cantley LC, Thompson CB. Understanding the Warburg effect: the metabolic requirements of cell proliferation. *Science*. 2009;324(5930):1029–1033.
2. Cantor JR, Sabatini DM. Cancer cell metabolism: one hallmark, many faces. *Cancer Discov*. 2012;2(10):881–898.
3. Ward PS, Thompson CB. Metabolic reprogramming: a cancer hallmark even warburg did not anticipate. *Cancer Cell*. 2012;21(3):297–308.
4. Metallo CM, et al. Reductive glutamine metabolism by IDH1 mediates lipogenesis under hypoxia. *Nature*. 2011;481(7381):380–384.
5. Mullen AR, et al. Reductive carboxylation supports growth in tumour cells with defective mito-

chondria. *Nature*. 2011;481(7381):385–388.
6. Gao P, et al. c-Myc suppression of miR-23a/b enhances mitochondrial glutaminase expression and glutamine metabolism. *Nature*. 2009;458(7239):762–765.
7. Wise DR, et al. Myc regulates a transcriptional program that stimulates mitochondrial glutaminolysis and leads to glutamine addiction. *Proc Natl Acad Sci U S A*. 2008;105(48):18782–18787.
8. Zadra G, Photopoulos C, Loda M. The fat side of prostate cancer. *Biochim Biophys Acta*. 2013;1831(10):1518–1532.
9. Rossi S, et al. Fatty acid synthase expression defines distinct molecular signatures in prostate cancer. *Mol Cancer Res*. 2003;1(10):707–715.
10. Fendt SM, et al. Metformin decreases glucose oxidation and increases the dependency of prostate cancer cells on reductive glutamine metabolism. *Cancer Res*. 2013;73(14):4429–4438.
11. Menendez JA, Lupu R. Fatty acid synthase and the lipogenic phenotype in cancer pathogenesis. *Nat Rev Cancer*. 2007;7(10):763–777.
12. Currie E, Schulze A, Zechner R, Walther TC, Farese RV, Farese RV Jr. Cellular fatty acid metabolism and cancer. *Cell Metab*. 2013;18(2):153–161.
13. Dasgupta S, Lonard DM, O'Malley BW. Nuclear receptor coactivators: master regulators of human health and disease. *Annu Rev Med*. 2014;65:279–292.
14. Chopra AR, et al. Absence of the SRC-2 coactivator results in a glycogenopathy resembling Von Gierke's disease. *Science*. 2008; 322(5906):1395–1399.
15. Chopra AR, et al. Cellular energy depletion resets whole-body energy by promoting coactivator-mediated dietary fuel absorption. *Cell Metab*. 2011;13(1):35–43.
16. Picard F, et al. SRC-1 and TIF2 control energy balance between white and brown adipose tissues. *Cell*. 2002;111(7):931–941.
17. Stashi E, et al. SRC-2 is an essential coactivator for orchestrating metabolism and circadian rhythm. *Cell Rep*. 2014;6(4):633–645.
18. Taylor BS, et al. Integrative genomic profiling of human prostate cancer. *Cancer Cell*. 2010;18(1):11–22.
19. Agoulnik IU, et al. Androgens modulate expression of transcription intermediary factor 2, an androgen receptor coactivator whose expression level correlates with early biochemical recurrence in prostate cancer. *Cancer Res*. 2006;66(21):10594–10602.
20. Dasgupta S, Srinidhi S, Vishwanatha JK. Oncogenic activation in prostate cancer progression and metastasis: molecular insights and future challenges. *J Carcinog*. 2012;11:4.
21. Duteil D, et al. The transcriptional coregulators TIF2 and SRC-1 regulate energy homeostasis by modulating mitochondrial respiration in skeletal muscles. *Cell Metab*. 2010;12(5):496–508.
22. Dasgupta S, Zhang B, Louet JF, O'Malley BW. Steroid receptor coactivator-2 mediates oncogenic reprogramming of cancer cell metabolism. *Cancer Res*. 2012;72:5153.
23. Price DT, Coleman RE, Liao RP, Robertson CN, Polascik TJ, DeGrado TR. Comparison of [18 F]fluorocholine and [18 F]fluorodeoxyglucose for positron emission tomography of androgen dependent and androgen independent prostate cancer. *J Urol*. 2002;168(1):273–280.
24. Kosaka T, Miyajima A, Nagata H, Maeda T, Kikuchi E, Oya M. Human castration resistant prostate cancer rather prefer to decreased 5α-reductase activity. *Sci Rep*. 2013;3:1268.
25. Liu AY, et al. Lineage relationship between LNCaP and LNCaP-derived prostate cancer cell lines. *Prostate*. 2004;60(2):98–108.
26. Yoo H, Antoniewicz MR, Stephanopoulos G, Kelleher JK. Quantifying reductive carboxylation flux of glutamine to lipid in a brown adipocyte cell line. *J Biol Chem*. 2008;283(30):20621–20627.
27. Zhang J, Ahn WS, Gameiro PA, Keibler MA, Zhang Z, Stephanopoulos G. 13C isotope-assisted methods for quantifying glutamine metabolism in cancer cells. *Methods Enzymol*. 2014;542:369–389.
28. Gameiro PA, et al. In vivo HIF-mediated reductive carboxylation is regulated by citrate levels and sensitizes VHL-deficient cells to glutamine deprivation. *Cell Metab*. 2013;17(3):372–385.
29. Wang Q, et al. A hierarchical network of transcription factors governs androgen receptor-dependent prostate cancer growth. *Mol Cell*. 2007;27(3):380–392.
30. Seo YK, Chong HK, Infante AM, Im SS, Xie X, Osborne TF. Genome-wide analysis of SREBP-1 binding in mouse liver chromatin reveals a preference for promoter proximal binding to a new motif. *Proc Natl Acad Sci U S A*. 2009;106(33):13765–13769.
31. Kim JB, et al. Nutritional and insulin regulation of fatty acid synthetase and leptin gene expression through ADD1/SREBP1. *J Clin Invest*. 1998;101(1):1–9.
32. Smolkova K, Jezek P. The role of mitochondrial NADPH-dependent isocitrate dehydrogenase in cancer cells. *Int J Cell Biol*. 2012;2012:273947.
33. Costello LC, Liu Y, Franklin RB, Kennedy MC. Zinc inhibition of mitochondrial aconitase and its importance in citrate metabolism of prostate epithelial cells. *J Biol Chem*. 1997;272(46):28875–28881.
34. Singh KK, Desouki MM, Franklin RB, Costello LC. Mitochondrial aconitase and citrate metabolism in malignant and nonmalignant human prostate tissues. *Mol Cancer*. 2006;5:14.
35. Duran RV, et al. Glutaminolysis activates Rag-mTORC1 signaling. *Mol Cell*. 2012;47(3):349–358.
36. Nicklin P, et al. Bidirectional transport of amino acids regulates mTOR and autophagy. *Cell*. 2009;136(3):521–534.
37. Han SJ, Lonard DM, O'Malley BW. Multi-modulation of nuclear receptor coactivators through posttranslational modifications. *Trends Endocrinol Metab*. 2009;20(1):8–15.
38. Kamphorst JJ, et al. Hypoxic and Ras-transformed cells support growth by scavenging unsaturated fatty acids from lysophospholipids. *Proc Natl Acad Sci U S A*. 2013;110(22):8882–8887.
39. Peterson TR, et al. mTOR complex 1 regulates lipin 1 localization to control the SREBP pathway. *Cell*. 2011;146(3):408–420.
40. Demirkan G, Yu K, Boylan JM, Salomon AR, Gruppuso PA. Phosphoproteomic profiling of in vivo signaling in liver by the mammalian target of rapamycin complex 1 (mTORC1). *PLoS One*. 2011;6(6):e21729.
41. Hsu PP, et al. The mTOR-regulated phosphoproteome reveals a mechanism of mTORC1-mediated inhibition of growth factor signaling. *Science*. 2011;332(6035):1317–1322.
42. Hanahan D, Weinberg RA. Hallmarks of cancer: the next generation. *Cell*. 2011;144(5):646–674.
43. Dasgupta S, O'Malley BW. Transcriptional coregulators: emerging roles of SRC family of coactivators in disease pathology. *J Mol Endocrinol*. 2014;53(2):R47–R59.
44. Shukla K, et al. Design, synthesis, and pharmacological evaluation of bis-2-(5-phenylacetamido-1,2,4-thiadiazol-2-yl)ethyl sulfide 3 (BPTES) analogs as glutaminase inhibitors. *J Med Chem*. 2012;55(23):10551–10563.
45. Jeong SM, et al. SIRT4 has tumor-suppressive activity and regulates the cellular metabolic response to DNA damage by inhibiting mitochondrial glutamine metabolism. *Cancer Cell*. 2013;23(4):450–463.
46. Sreekumar A, et al. Metabolomic profiles delineate potential role for sarcosine in prostate cancer progression. *Nature*. 2009;457(7231):910–914.
47. DeBerardinis RJ, et al. Beyond aerobic glycolysis: transformed cells can engage in glutamine metabolism that exceeds the requirement for protein and nucleotide synthesis. *Proc Natl Acad Sci U S A*. 2007;104(49):19345–19350.
48. Csibi A, et al. The mTORC1 pathway stimulates glutamine metabolism and cell proliferation by repressing SIRT4. *Cell*. 2013;153(4):840–854.
49. Igal RA. Stearoyl-CoA desaturase-1: a novel key player in the mechanisms of cell proliferation, programmed cell death and transformation to cancer. *Carcinogenesis*. 2010;31(9):1509–1515.
50. Makhov P, Golovine K, Uzzo RG, Wuestefeld T, Scoll BJ, Kolenko VM. Transcriptional regulation of the major zinc uptake protein hZip1 in prostate cancer cells. *Gene*. 2009;431(1):39–46.
51. Gehin M, Mark M, Dennefeld C, Dierich A, Gronemeyer H, Chambon P. The function of TIF2/GRIP1 in mouse reproduction is distinct from those of SRC-1 and p/CIP. *Mol Cell Biol*. 2002;22(16):5923–5937.
52. Putluri N, et al. Metabolomic profiling reveals a role for androgen in activating amino acid metabolism and methylation in prostate cancer cells. *PLoS One*. 2011;6(7):e21417.
53. Subramanian A, et al. Gene set enrichment analysis: a knowledge-based approach for interpreting genome-wide expression profiles. *Proc Natl Acad Sci U S A*. 2005;102(43):15545–15550.